## Accepted Article

**Authors:** Simon J. Pope, Christopher E. Elgar, Haleema Y. Otaif, Xue Zhang, Jianzhang Zhao, Joseph M. Beames, Peter N. Horton, and Simon J. Coles

**WILEY-VCH**

# Iridium(III) Sensitizers and Energy Upconversion: The Influence of Ligand Structure Upon TTA-UC Performance

Christopher E. Elgar,‡[a] Haleema Y. Otaif,‡[a] Xue Zhang,‡ [b] Jianzhang Zhao,[b] Peter N. Horton,[c] Simon J. Coles,[c] Joseph M. Beames,*[a] and Simon J.A. Pope*[a]

[a]School of Chemistry, Main Building, Cardiff University, Cardiff CF10 3AT, Cymru/Wales, UK; [b] State Key Laboratory of Fine Chemicals Dalian University of Technology, Dalian 116024 (P.R. China); [c]UK National Crystallographic Service, Chemistry, Faculty of Natural and Environmental Sciences, University of Southampton, Highfield, Southampton, SO17 1BJ, England, UK.
Email: popesj@cardiff.ac.uk; beamesj@cardiff.ac.uk

‡ equal contributions

## Abstract

Six substituted ligands based upon 2-(naphthalen-1-yl)quinoline-4-carboxylate and 2-(naphthalen-2-yl)quinoline-4-carboxylate have been synthesized in two steps from a range of commercially available isatin derivatives. These species are demonstrated to be effective cyclometalating ligands for Ir(III), yielding complexes of the form $[Ir(C^\wedge N)_2(bipy)]PF_6$ (where $C^\wedge N$ = cyclometalating ligand; bipy = 2,2'-bipyridine). X-ray crystallographic studies on three examples demonstrate that the complexes adopt a distorted octahedral geometry wherein a *cis*-C,C and *trans*-N,N coordination mode is observed. Intra-ligand torsional distortions are evident in all cases. The Ir(III) complexes display photoluminescence in the red part of the visible region (668-693 nm) which is modestly tuneable via the ligand structure. The triplet lifetimes of the complexes are clearly influenced by the precise structure of the ligand in each case. Supporting computational (DFT) studies suggest that the differences in observed triplet lifetime are likely due to differing admixtures of ligand-centred *versus* MLCT character instilled by the facets of the ligand structure. Triplet-triplet annihilation upconversion (TTA-UC) measurements demonstrate that the complexes based upon the 1-naphthyl derived ligands are viable photosensitizers with upconversion quantum efficiencies of 1.6-6.7 %.

1

**Introduction**

Luminescent cyclometalated iridium(III) complexes are of major interest in optoelectronic and photonic applications.[1] Such complexes have demonstrated applications in research fields including bioimaging,[2] electroluminescence,[3] photoredox catalysts,[4] non-linear optics,[5] and chemosensors.[6] An intimate understanding of the electronic characteristics of the complex[7] can provide control over the luminescence properties of these species and, thus, careful consideration of the ligand design is highly desirable to maximise their applicability.[8]

The use of transition metal complexes as photosensitizers for energy upconversion processes has also gathered increasing attention over the last decade.[9] In particular, the use of triplet sensitizers via a triplet-triplet annihilation (TTA) mechanism has led to several studies on TTA upconversion (TTA-UC). This is a bimolecular process that requires energy transfer between a sensitizer and an annihilator species. As the Dexter energy transfer mechanism requires collisional interactions, a long-lived excited state triplet lifetime is clearly advantageous. Therefore, a variety of metal-based photosensitizers have been investigated in this regard.

Castellano and co-workers have reported several important studies that demonstrate the utility of phosphorescent metal complexes in TTA-UC. Early work described the use of the classical metal-to-ligand charge transfer (MLCT) species $[Ru(dmb)_3]^{2+}$ (dmb = 4,4,dimethyl-2,2'-bipyridine) as a photosensitizer for solution-based TTA-UC with 9,10-diphenylanthracene (DPA) as the annihilator species.[10] The ease with which luminescent complexes can be functionalised, whilst retaining their inherent photophysical attributes, has been demonstrated in the development of a water soluble Ru(II) analogue, a bathophenanthroline disulfonate variant of $[Ru(N^{\wedge}N)_3]^{2+}$, which was successfully utilised as a triplet photosensitiser for TTA-UC under aqueous conditions.[11] To optimise the photosensitizer absorption characteristics, a multi-component system comprising a NIR absorbing Ru(II) complex unit conjugated with a dimetallic Zn(II) di-porphyrin chromophore was developed, which displayed TTA-UC when used in conjunction with a *N,N*-bis(ethylpropyl)perylene-3,4,9,10-tetracarboxylicdiimide or tetracene annihilator species.[12] Importantly, earth abundant Cu(I) MLCT phosphorescent species based

2

on substituted 1,10-phenanthroline ligands have also been studied as viable photosensitizers for TTA-UC.[13]

Organometallic iridium(III) complexes have also shown excellent application in TTA-UC, benefiting from attributes such as good photostability, efficient intersystem crossing (ISC) and long triplet lifetimes.[14] Ma and co-workers have described a number of energy upconverting systems, including tethered systems, based on tris-cyclometalated Ir(III) photosensitizers with 2-phenylpyridine (ppy) type ligands.[15,16] Some of the iridium-pyrene bichromophoric systems benefit from remarkable millisecond triplet lifetimes, which enhances TTA-UC.[16a] Zhao and co-workers have also reported a significant number of TTA-UC studies that exploit and optimise the properties of Ir(III) photosensitizers.[17] These include strategies to address the visible light absorption characteristics, and elongate the excited state triplet lifetimes of the photosensitizer species.

Our own contribution to the area reported a series of cationic Ir(III) complexes as triplet sensitizers which have shown the highest yet reported TTA-UC efficiency of 39% using DPA as the annihilator.[18] These Ir(III) sensitizer complexes were based upon a 2-phenylquinoxaline ligand framework, [19,20] which impart good absorption characteristics in the visible region. Because of the increase in conjugation of the chelating ligands, these characteristics also provide bathochromically shifted emission compared to the ubiquitous Ir(III) complexes based on ppy.[21,22]

Indeed, red-emitting Ir(III) species are attracting significant attention, being applicable to a number of other optoelectronic applications. A common strategy for red-shifting the emission wavelengths of Ir(III) species is to increase the conjugation of the chelating ligands. As an example, comparing [Ir(ppy)$_3$] *versus* [Ir(piq)$_3$]) (ppy = 2-phenylpyridine; piq = 1-phenylisoquinoline) shows a bathochromic shift in the emission for the latter to around 620 nm.[23] Relatively simple evolutions of this design strategy can provide further extensions of $\lambda_{em}$ into the near-IR (>750 nm) region.[24] Of course, previous studies have investigated a variety of different aryl groups as components of cyclometalating C^N ligands, including early, seminal[25] studies on luminescent Ir(III) complexes.[26] Other recent examples of red phosphorescence from Ir(III) species have been achieved through the use of conjugated triazole,[27] conjugated phenazine,[28] and cyclometalating phenylquinazoline[29] ligands. Teets and co-workers have also described a systematic study of a series of anionic ancillary

3

ligands which facilitate excellent control over the emitting state energies of their Ir(III) complexes.[30] The addition of bulky groups to the ancillary ligand was shown as a useful strategy for improving the quantum yields of these deep red phosphorescing species. We have also reported the use of substituted 2-phenylquinoline[31] cyclometalating (C^N) ligands for red emitting Ir(III) complexes. It is noteworthy that red-emitting luminophores are important in bioimaging disciplines which use confocal fluorescence microscopy techniques.[32]

Herein we report the photophysical properties of a series of new [Ir(C^N)$_2$(bipy)]PF$_6$ complexes formed from substituted 2-(naphthalen-1-yl)quinoline-4-carboxylate and 2-(naphthalen-2-yl)quinoline-4-carboxylate as cyclometalating ligands. Of direct relevance to the current study, Li *et al* have previously investigated the influence of $\pi$-conjugation in unsubstituted naphthyl-pyridine type ligands upon the non-linear absorbing properties of a series of Ir(III) complexes;[33] the complexes luminesce in the yellow-orange region with some noted photophysical differences that result from the isomeric form of the ligand. In our current work, we show that a new naphthylquinoline ligand framework can further bathochromically shift the absorption and emission properties of the Ir(III) complexes, and several species have potential application as photosensitizers in TTA-UC.

4

## Results and Discussion

## Synthesis and characterization of the ligands

The synthesis of the ligands was achieved using the Pfitzinger[34] reaction, which dates back to the 1880s.[35,36] This reaction involves aryl acetyl and isatin reagents and provides a convenient and efficient synthetic route towards substituted 2-aryl-quinoline-4-carboxylic acids. Presently, 1-acetylnaphthalene and 2-acetylnaphthalene were employed as the aryl acetyl reagent; each was reacted with three different, commercially available isatins (isatin, 5-methoxyisatin and 5-fluoroisatin) to yield the subsequent 2-(naphthyl)quinoline-4-carboxylic acids. These carboxylic acid derivatives were then esterified to improve solubility in common organic solvents (Scheme 2).

For **LH¹** and **LH⁴** and their corresponding carboxylic acids ¹H NMR data was consistent with the formulation of these previously reported compounds.[37] Finally, to optimize solubility for the subsequent Ir(III) coordination chemistry, the carboxylic acids were esterified to give 2-(naphthalen-2-yl)quinoline-4-carboxylic esters, **LH¹**, **LH²** and **LH³** (where R = H, OMe and F, respectively), and 2-(naphthalen-1-yl)quinoline-4-carboxylic esters, **LH⁴**, **LH⁵** and **LH⁶** (where R = H, OMe and F, respectively). Thus, a series of structurally related, disubstituted ligands were conveniently isolated in two synthetic steps (Scheme 1).

<Scheme 1>

All new ligands were fully characterised using a range of standard methods. ¹H and ¹³C{¹H} NMR spectroscopies were consistent with the proposed formulations. For **LH³** and **LH⁶**, ¹⁹F{¹H} NMR was also used showing resonances at -110.4 and -109.9 ppm, respectively. Satisfactory HRMS data was obtained for each new esterified ligand.

## Coordination chemistry

The six ligands (**LH¹⁻⁶**) were then explored as cyclometalating (C^N) agents for Ir(III). The adopted approach for the Ir(III) precursor utilized standard reaction conditions based upon those first reported by Nonoyama[38] wherein reaction with hydrated IrCl₃ proceeds to the dimeric species, [{Ir(C^N)₂(μ-Cl)}₂]. The target monometallic Ir(III)

5

complexes [Ir(C^N)$_2$(bipy)]PF$_6$ were then synthesised *via* the intermediate species *cis*-[Ir(MeCN)$_2$(C^N)$_2$]BF$_4$. All complexes (Scheme 2) were obtained as red coloured, air-stable powders following chromatographic purification on silica gel (see Experimental Section, SI).

<Scheme 2>

**Characterization of the Complexes**

^{1}H NMR spectroscopic studies on the complexes showed shifts in the aromatic protons of the ligands that were indicative of chelation. Firstly, the ^{1}H NMR spectrum of the reaction product with **LH$^2$** indicated quantitative conversion to the ethoxyethanol ester analogue (supported by four resonances in the ^{13}C NMR spectrum at 70-55 ppm). The indicative transesterification in 2-ethoxyethanol solvent at elevated temperatures has been observed previously, and the resultant complex product is thus labelled [Ir(**L$^{2b}$**)$_2$(bipy)]PF$_6$ (Scheme 2).[39] In each complex, a relatively upfield resonance between *ca.* 6.9 and 7.0 ppm was noted for the proton adjacent to the cyclometalated carbon atom. Both [Ir(**L$^{2b}$**)$_2$(bipy)]PF$_6$ and [Ir(**L$^5$**)$_2$(bipy)]PF$_6$ have an additional upfield signal at 6.58 and 6.60 ppm respectively. Using [1]H-[1]H Correlation Spectroscopy on [Ir(**L$^{2b}$**)$_2$(bipy)]PF$_6$ (Fig. S1), this was assigned to the proton on C7 of the quinoline ring, which is adjacent to the methoxy group. In the cases of [Ir(**L$^{2b}$**)$_2$(bipy)]PF$_6$ and [Ir(**L$^5$**)$_2$(bipy)]PF$_6$ the methoxy substituent appears *ca.* 4 ppm.

For [Ir(**L$^3$**)$_2$(bipy)]PF$_6$ and [Ir(**L$^6$**)$_2$(bipy)]PF$_6$, ^{19}F{^{1}H} NMR spectra were also obtained (Table S1), firstly showing the doublet ($^1J_{FP}$) feature associated with the hexafluorophosphate anion at -72.6 ppm, and secondly, a resonance around -107.5 ppm attributed to the fluorine substituent of the quinoline ring. The latter represents a subtle downfield shift upon coordination of the ligand to the Ir(III) centre.

HRMS data were obtained for all six complexes showing the correct isotopic distribution for the complex cation in each case. For [Ir(**L$^{2b}$**)$_2$(bipy)]PF$_6$ the MS data again supported the isolation of the ethoxyethanol ester as evidenced by the NMR studies.

6

(

## X-ray Crystallographic Studies

Single, red plate-shaped crystals from three of the complexes, [Ir(**L³**)$_2$(bipy)]PF$_6$, [Ir(**L⁴**)$_2$(bipy)]PF$_6$, and [Ir(**L⁶**)$_2$(bipy)]PF$_6$, were successfully isolated from vapour diffusion of diethyl ether into an acetonitrile solution of the complex, and investigated using X-ray diffraction. Although of lower quality, the data for [Ir(**L⁶**)$_2$(bipy)]PF$_6$ was still sufficient to allow determination of the key features of the structure and is also included here. Data collection parameters are in Table S2 (SI); selected bond lengths and bond angles associated with the coordination spheres are in Table S3 (SI). In each case the structures confirmed the anticipated coordination sphere at iridium, with the 2-(naphthalen-1-yl)quinoline-4-carboxylate and 2-(naphthalen-2-yl)quinoline-4-carboxylate derived ligands coordinating in the expected cyclometalating fashion. Hypothetically, there are two available sites of cyclometalation for the 2-(naphthalen-2-yl)quinoline-4-carboxylate ligand. The structure of [Ir(**L³**)$_2$(bipy)]PF$_6$ shows the ligand coordinates at the 3 position of the naphthyl ring. The reaction conditions employed here are known to promote the *cis*-C,C and *trans*-N,N coordination mode of cyclometalation at Ir(III), which was confirmed in all three structures.[40] [Ir(**L³**)$_2$(bipy)]PF$_6$ also shows disorder over one of the ethoxy groups on the ligand backbone.

A comparison of the Ir-C bond lengths suggests that there is little influence from the particular isomeric form of the naphthyl donor, and the Ir-C and Ir-N bond lengths are closely comparable to other relevant examples.[19] In all cases significant distortions from ideal octahedral geometry are noted, with ∠N−Ir−N bond angles, that originate from the *trans*-N,N arrangement, of 172.09(10), 174.57(12) and 175.2(4)° for [Ir(**L³**)$_2$(bipy)]PF$_6$, [Ir(**L⁴**)$_2$(bipy)]PF$_6$, and [Ir(**L⁶**)$_2$(bipy)]PF$_6$, respectively. Intra-ligand distortions are also noted, with appreciable torsion angles between the naphthyl and quinoline rings of the cyclometalating ligands, particularly for [Ir(**L⁴**)$_2$(bipy)]PF$_6$.

<Figure 1>

<Figure 2>

<Figure 3>

7

.

The Continuous Shape Measures (CShM) software[41] was used to evaluate the polyhedral environment around the iridium ion and its deviation from an ideal octahedron. The lowest CShM values define the best ideal polyhedron; values > 0.1 are considered chemically significant distortions, while > 3 indicate important distortions. For these three complexes, the values against an ideal octahedron are as follows: 1.952, 1.915, 1.619 for [Ir(**L$^3$**)$_2$(bipy)]PF$_6$, [Ir(**L$^4$**)$_2$(bipy)]PF$_6$ [Ir(**L$^6$**)$_2$(bipy)]PF$_6$, respectively. Thus, although [Ir(**L$^3$**)$_2$(bipy)]PF$_6$ has a different isomeric form of ligand, it does not lead to a major comparative distortion.

## Redox properties of the Ir(III) complexes

The electrochemical characteristics of the complexes were studied in deoxygenated dichloromethane. The cyclic voltammograms (Fig. S2) were measured using a platinum disc electrode (scan rate $\upsilon$ = 200 mV s$^{-1}$, 1 × 10$^{-3}$ M solutions, 0.1 M [NBu$_4$][PF$_6$] as a supporting electrolyte). Each complex showed one fully reversible oxidation (Table 1) at +1.26 to +1.39 V which is ascribed to the Ir$^{3+/4+}$ couple. The small differences in oxidation potential are likely due to two factors: the isomeric form of the cyclometalating unit (2-naphthyl *vs.* 1-naphthyl), and the substitutent (H *vs.* OMe *vs.* F) on the quinoline ring; both factors may influence the electron density at the iridium centre. For a given ligand substituent, the 1-naphthyl derived complexes showed a slightly higher Ir$^{3+/4+}$ potential. For a given naphthyl isomer, the methoxy-substituted complexes possess the lowest Ir$^{3+/4+}$ potentials suggesting that the Ir$^{3+}$ is more easily oxidisable, whereas fluorinated complexes with the highest $E_{ox}$ values, consistent with a more electron deficient quinoline ligand. The 1-naphthyl derivatives [Ir(**L$^{4-6}$**)$_2$(bipy)]PF$_6$ also showed two fully reversible reductions which were attributed to one-electron, ligand-centred processes. These reduction features also varied according to the nature of the substituent implying that both processes may be associated with the cyclometalated ligand. The 2-naphthyl variants [Ir(**L$^{1,2b,3}$**)$_2$(bipy)]PF$_6$ appeared less electrochemically stable with non-reversible features within the reduction couples.

8

|

**Table 1**. Electrochemical properties of the iridium(III) complexes obtained from cyclic voltammetry.[a]

| Complex | Oxidation | Reduction | |
|---|---|---|---|
| | $E_{1/2}$ / V | $E_{(red\ 1)}$ / V | $E_{(red\ 2)}$ / V |
| $[Ir(L^1)_2(bipy)]PF_6$ | +1.28 | -1.10[b] | -1.27[b] |
| $[Ir(L^{2b})_2(bipy)]PF_6$ | +1.26 | -1.14[b] | -1.31[b] |
| $[Ir(L^3)_2(bipy)]PF_6$ | +1.32 | -0.93[b] | -1.21[b] |
| $[Ir(L^4)_2(bipy)]PF_6$ | +1.37 | -1.05[c] | -1.29[c] |
| $[Ir(L^5)_2(bipy)]PF_6$ | +1.29 | -1.11[c] | -1.33[c] |
| $[Ir(L^6)_2(bipy)]PF_6$ | +1.39 | -0.97[c] | -1.22[c] |

[a] potentials measured in $CH_2Cl_2$ solutions at 200 mVs$^{-1}$ with 0.1 M [NBu$_4$][PF$_6$] as supporting electrolyte calibrated with Fc/Fc$^+$; [b] cathodic peak of irreversible process; [c] $E_{1/2}$ values for fully reversible process.

## Density functional theory (DFT)

Discussion below focuses on two of the complexes that represent the key isomeric variants within the series, $[Ir(L^1)_2(bipy)]^+$ and $[Ir(L^4)_2(bipy)]^+$. These were optimized in their lowest electronic singlet and triplet states at the DFT//B3LYP/6-31G* level of theory, with an implicit $CH_3CN$ solvent (IEFPCM). The optimized geometries of both complexes obtained by DFT method were confirmed through harmonic vibrational frequency calculations and are shown in Fig. S3. The modelled structures exhibit near $C_2$ symmetry, with a distorted octahedral geometry around the iridium metal center. The DFT-derived optimized bond lengths and angles are in good agreement with the X-ray experimental data, with typically less than 0.05 Å (bond distances) and 1° (bond angles) difference between optimized geometric parameters and those derived from experiment (Table S4). It is worth noting that the DFT bond lengths are typically longer than those reported in the X-ray crystal structure(s).

9

Molecular orbital decomposition analysis (Tables 2, 3 and 4) indicates that the HOMO for both Ir(III) complexes is made predominantly of contributions from the naphthyl moiety of both C^N ligands, and a significant, but smaller contribution from the iridium centre. For example, in the case of the 2-naphthyl derivative [Ir(**L$^1$**)$_2$(bipy)]$^+$, the HOMO is mainly localized over the π-orbitals of the naphthyl moiety of both C^N ligands (36%, 34%) and the 5d-orbitals of Ir(III) (28%), with just a 2% contribution from the bipyridine. The prediction, that a metal $d$-orbital contribution to the HOMO is less than ligand contributions is similar to other Ir(III) quinoxaline systems reported previously. The 1-naphthyl derivative [Ir(**L$^4$**)$_2$(bipy)]$^+$ also predicts an Ir contribution to the HOMO of 21%, with equal contributions from naphthyl moieties on both C^N ligands (39%). The HOMO-1 of the two complexes is divided between the naphthyl moieties of both ligands (around 49%) and a negligible contribution from the metal centre (≤ 3%).

In both cases, the LUMO is predicted to reside predominantly on the quinoline part of the C^N ligands. It is noticeable that the two ligands form pairs of pseudo-degenerate orbitals with alternating contributions from each of the C^N ligands: *e.g.* the [Ir(**L$^1$**)$_2$(bipy)] LUMO is comprised of contributions of 26% and 71% from the quinolines, Q1 and Q2 respectively, whilst the LUMO+1 shows the reverse (Q1 = 71%; Q2 = 26%). This effect is due to the near $C_2$ symmetry of the system, with subtle geometrical distortions leading to a lowering of the total symmetry and thus a splitting in the orbitals. The metal center and bipyridine make little contribution to the LUMO or LUMO+1; it is only in the higher energy LUMO+2 that a dominant contribution (97%) of the bipyridine ligand is predicted. The full list of calculated MO contributions and excited state descriptions and associated transitions for all of the complexes are presented in the Supplementary Information (Tables S5-S15).

TD-DFT was used in conjunction with the long-range corrected CAM-B3LYP functional to investigate the predicted UV-Vis electronic transitions of these complexes. All calculations were performed from the optimized ground state singlet (S$_0$) and lowest triplet (T$_1$) state geometries. The calculated transition energies are in reasonable agreement with the experimental UV-Vis absorption spectra discussed later (Fig. 4). The lowest spin-forbidden singlet-triplet transition is predicted to occur at 570 nm for [Ir(**L$^1$**)$_2$(bipy)]$^+$, attributed to a $^3$MLCT contribution, and correlates well

10

with low intensity absorption tail at 550 nm in the experimental absorption spectra. The lowest singlet excited state is predicted to be an intense HOMO to LUMO transition at 407 nm, followed at higher energy by an intense HOMO to LUMO+1 transition at 402 nm (f = 0.0375), both of which suggest a combination of $^1$MLCT and C^N ligand-centered character. These transitions are in good agreement with the experimental absorption bands at ca. 350 nm < $\lambda$ < 425 nm. The TD-DFT also predicts intense transitions between 350 nm < $\lambda$ < 300 nm, including transitions with much more mixed $^1$ILCT/$^1$LLCT/$^1$MLCT character. In general, as one moves to shorter wavelength (higher energy), the TD-DFT calculations suggest an increase in ligand-centered transitions, as might be expected for quinoline, which has unperturbed UV-Vis band onsets at ca. 310 nm. The simulations for [Ir(**L$^4$**)$_2$(bipy)]$^+$ predict (see also Table S12, SI) similar features albeit with a bathochromic shift compared to [Ir(**L$^1$**)$_2$(bipy)]$^+$; again this is supported by the experimental data discussed later.

11

**Table 2.** Calculated Kohn-Sham molecular orbitals for [Ir($L^1$)$_2$(bipy)]$^+$. Calculated spin densities are reported in the SI (Fig. S4 and Table S5).

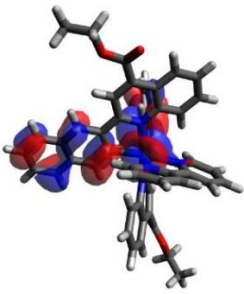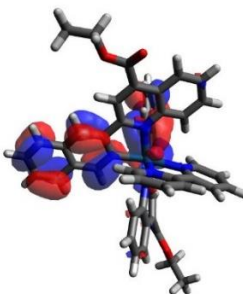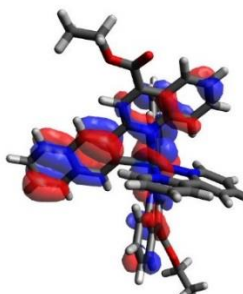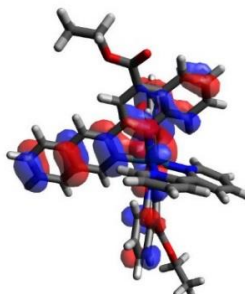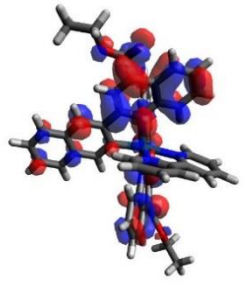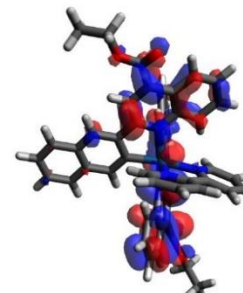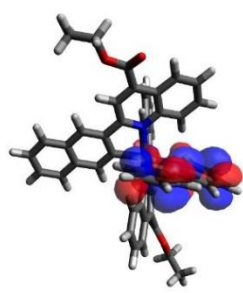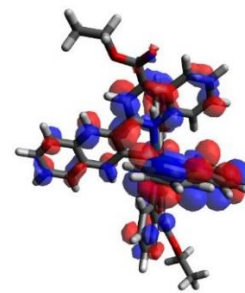| HOMO | HOMO-1 | HOMO-2 | HOMO-3 |
|---|---|---|---|
|  |  |  |  |
| LUMO | LUMO+1 | LUMO+2 | LUMO+3 |
|  |  |  |  |

**Table 3.** A description of the calculated MO contributions, excited state descriptions and their associated transitions for [Ir($L^1$)$_2$(bipy)]X (Q1 and Q2 are the different naphthylquinoline ligands; bipy = bipyridine).

| Orbital | Moiety Contribution to Orbital (%) | | | | Orbital Contribution to Excited State | |
|---|---|---|---|---|---|---|
| | Ir (5d) | bipy | Q1 | Q2 | Excited State | Contributing Transitions (> 10%) |
| **LUMO +4** | 1 | 23 | 17 | 59 | 1 (407 nm  f=0.0039) | HOMO → LUMO (83.84%) |
| **LUMO +3** | 1 | 44 | 26 | 29 | | |
| **LUMO +2** | 2 | 97 | 1 | 1 | 2 (403 nm  f=0.0375) | HOMO → LUMO +1 (82.53%) |
| **LUMO +1** | 3 | 0 | 71 | 26 | | |
| **LUMO** | 2 | 1 | 26 | 71 | | |
| **HOMO** | 28 | 2 | 36 | 34 | 3 (356 nm  f=0.4075) | HOMO -2 → LUMO +1 (22.16%) |
| **HOMO -1** | 3 | 1 | 48 | 49 | | HOMO -1 → LUMO (31.29%) |
| **HOMO -2** | 10 | 0 | 45 | 45 | 4 (352 nm  f=0.3415) | HOMO -2 → LUMO (31.29%) |
| **HOMO -3** | 9 | 1 | 45 | 45 | | HOMO -1 → LUMO +1(40.03%) |
| **HOMO -4** | 41 | 5 | 35 | 19 | 5 (344 nm  f=0.0015) | HOMO → LUMO+2 (84.16%) |

12

**Table 4.** A description of the calculated MO contributions, excited state descriptions and their associated transitions for [Ir(**L⁴**)₂(bipy)]⁺ (Q1 and Q2 are the different quinoline ligands; bipy = bipyridine).

| Orbital | Moiety Contribution to Orbital (%) | | | | Orbital Contribution to Excited State | |
|---|---|---|---|---|---|---|
| | Ir (5d) | Bipy | Q1 | Q2 | Excited State | Contributing Transitions (> 10%) |
| **LUMO +4** | 2 | 6 | 46 | 46 | 1 (432 nm f=0.1466) | HOMO-1 → LUMO (11.70%) |
| **LUMO +3** | 2 | 23 | 34 | 41 | | HOMO → LUMO (63.65%) |
| | | | | | | HOMO → LUMO +1 (11.52%) |
| **LUMO +2** | 2 | 97 | 1 | 1 | 2 (430 nm f=0.1722) | HOMO -1 → LUMO+1 (11.03%) |
| **LUMO +1** | 4 | 1 | 79 | 17 | | HOMO → LUMO (12.50%) |
| **LUMO** | 4 | 1 | 16 | 78 | | HOMO → LUMO +1 (62.32%) |
| **HOMO** | 21 | 1 | 39 | 39 | 3 (350 nm f=0.1746) | HOMO -2 → LUMO+1 (11.62%) |
| **HOMO -1** | 2 | 0 | 49 | 49 | | HOMO -1 → LUMO (50.34%) |
| **HOMO -2** | 16 | 1 | 42 | 41 | | HOMO → LUMO +2 (13.23%) |
| **HOMO -3** | 37 | 4 | 51 | 8 | 4 (347 nm f=0.1456) | HOMO -2 → LUMO (14.66%) |
| | | | | | | HOMO -1 → LUMO +1 (58.09%) |
| **HOMO -4** | 36 | 2 | 10 | 52 | 5 (343 nm f=0.0480) | HOMO → LUMO+2 (70.56%) |

TD-DFT was also used to compute the vertical and adiabatic spin-forbidden $T_1 \rightarrow S_o$ emission energies from the triplet state minimum energy geometries (Table S16). These calculations suggest that phosphorescence bands should exist at long wavelengths ($\lambda$ = 649 nm and 705 nm for [Ir(**L¹**)₂(bipy)]⁺ and [Ir(**L⁴**)₂(bipy)]⁺, respectively) which is in good qualitative agreement with the experimental data; the band positions are overestimated for the calculated adiabatic emission profiles. As with the $S_o \rightarrow T_n$ absorption, this band is predicted as possessing some ³MLCT character. The molecular orbital decomposition analyses shows that the contribution of the iridium to the HOMO orbital may be subtly dependent upon the nature of the C^N ligand.[42]

**Absorption and Emission properties of the Ir(III) complexes**

UV-vis. absorption spectra were obtained on MeCN solutions of the complexes. The spectra (Fig. 4) reveal a composite of bands between 220-550 nm. Ligand centered bands from the various aromatic components are anticipated to contribute to the more intense absorptions between 220-400 nm. Previous studies on related Ir(III) complexes suggest that spin allowed metal-to-ligand charge transfer (¹MLCT) absorptions contribute at 350-450 nm with spin forbidden absorptions to ³MLCT

13

excited states likely to result weaker features >450 nm.[18] The complexes herein demonstrate a similar pattern where the MLCT absorptions tail to around 600 nm, which is attributed to the extended conjugation of the cyclometalating ligands. Within the series it is clear that [Ir(**L$^{4-6}$**)$_2$(bipy)]PF$_6$ possess relatively bathochromically shifted MLCT features compared to [Ir(**L$^{1,2b,3}$**)$_2$(bipy)]PF$_6$. This is consistent with the predictions from the DFT calculations. Within these structural variants, the addition of substituents (H *vs.* OMe *vs.* F) to the quinoline ring induces only minor changes in the position of these absorption bands (Table 5).

**Table 5**. Absorbance and emission data for the complexes in aerated MeCN at room temperature.[a]

| Complex | $\lambda_{abs}$ ($\varepsilon \times 10^4$ M$^{-1}$ cm$^{-1}$) / nm[a] | $\lambda_{em}$ / nm[b] | $\tau$ /ns[c] | $\phi$ / %[d] |
|---|---|---|---|---|
| [Ir(L$^1$)$_2$(bipy)]PF$_6$ | 464 (0.2), 365 (2.9), 315 (3.3), 283 (5.4), 265 (6.6), 218 (7.4) | 673 | 36 | 0.3 |
| [Ir(L$^{2b}$)$_2$(bipy)]PF$_6$ | 480 (0.2), 401 (1.6), 367 (1.7), 321 (3.5), 280 (4.9), 221 (5.7) | 668 | 89 | 0.4 |
| [Ir(L$^3$)$_2$(bipy)]PF$_6$ | 483 (0.2), 399 (1.6), 365 (2.1), 268 (5.5) | 675 | 17 | 0.3 |
| [Ir(L$^4$)$_2$(bipy)]PF$_6$ | 494 (0.5), 405 (1.4), 366 (2.0), 271 (9.2) | 679 | 240 | 0.6 |
| [Ir(L$^5$)$_2$(bipy)]PF$_6$ | 495 (0.6), 417 (1.2), 367 (2.1), 267 (5.0), 223 (7.6) | 693 | 223 | 0.2 |
| [Ir(L$^6$)$_2$(bipy)]PF$_6$ | 492 (0.5), 408 (1.3), 367 (2.2), 264 (5.0), 216 (8.2) | 687 | 217 | 1.0 |

[a] aerated acetonitrile, 10$^{-5}$ M; [b] $\lambda_{ex}$ = 510 nm; [c] $\lambda_{ex}$ = 295 nm; [d] Quantum yield with [Ru(bipy)$_3$][PF$_6$]$_2$ as standard ($\Phi_\Delta$ = 0.018 in acetonitrile).[43]

<Figure 4>

Aerated MeCN solutions (10$^{-5}$ M) of the complexes were used to obtain photophysical data (Table 5). Following irradiation at 510 nm (*i.e.* in the region of the MLCT absorption bands) each of the complexes demonstrated emission in the deep red region of the spectrum, peaking at 668-693 nm and tailing to 800 nm (Fig. 5). The combination of the naphthyl and quinoline units within the C^N ligand framework leads to a significant bathochromic shift in emission wavelength when compared to either phenyl-quinoline or naphthyl-pyridine type systems reported by Sun and co-workers.[38] The peak appearances of [Ir(**L$^{4-6}$**)$_2$(bipy)]PF$_6$ were broad and featureless, but for [Ir(**L$^{1,2b,3}$**)$_2$(bipy)]PF$_6$ the higher energy portion of the peak possessed some

14

weaker vibronic features. Corresponding excitation spectra were also recorded and showed a close matching with the absorption spectral profiles (Fig. S5). The data suggests that the emitting state of the complexes can be populated *via* both MLCT and LC excited states.

As predicted by the DFT calculations, the 1-naphthyl species, [Ir(**L**$^{4-6}$)$_2$(bipy)]PF$_6$, were the most bathochromically shifted with subtle variations in $\lambda_{em}$ according to the presence of the different quinoline substituents (H *vs.* OMe *vs.* F). Under aerated conditions the observed lifetimes were significantly longer for the [Ir(**L**$^{4-6}$)$_2$(bipy)]PF$_6$ species (217-240 ns) compared to [Ir(**L**$^{1,2b,3}$)$_2$(bipy)]PF$_6$ (17-89 ns). The emission spectra were also collected in a range of solvents of varying polarity (Fig. S6). The results suggest that the excited states of the complexes are relatively insensitive to the polarity of the medium, unlike a classical MLCT species such as [Ru(bipy)$_3$]$^{2+}$.[43] Therefore in an admixture of LC and MLCT excited states the latter is unlikely to be the dominant contribution in these complexes.

<Figure 5>

Low temperature measurements (77 K) of each complex were also obtained (Fig. 6) using frozen glasses (4:1, EtOH:MeOH). For [Ir(**L**$^{1,2b,3}$)(bipy)]PF$_6$ the dominant peak maxima were hypsochromically shifted from the room temperature spectra and characterized by stronger vibronic structure, suggesting the possibility of a ligand-centered contribution to the emitting states. Interestingly, for the fluoro-substituted species, [Ir(**L**$^3$)(bipy)]PF$_6$, the peak appearance was broadened. In comparison, the spectra for [Ir(**L**$^{4-6}$)(bipy)]PF$_6$ presented a well-defined peak maximum at 650-675 nm with a much weaker shoulder feature to longer wavelength. Evidently, the vibronic features in [Ir(**L**$^{1,2b,3}$)(bipy)]PF$_6$ were stronger than for [Ir(**L**$^{4-6}$)(bipy)]PF$_6$. The onset of the low temperature steady state emission spectra give an approximation of the triplet energy levels of the Ir(III) complexes. Using this approach the triplet levels of [Ir(**L**$^{1,2b,3}$)(bipy)]PF$_6$ are *ca.* 17900 cm$^{-1}$ and those of [Ir(**L**$^{4-6}$)(bipy)]PF$_6$ are *ca.* 16400 cm$^{-1}$ (see later discussion). The emission lifetimes obtained at 77 K for [Ir(**L**$^{1,2b,3}$)$_2$(bipy)]PF$_6$ were extended to *ca.* 12 $\mu$s, but for [Ir(**L**$^{4-6}$)$_2$(bipy)]PF$_6$ they were *ca.* 3 $\mu$s. These observations, again, may point to differing and subtle admixtures of LC/MLCT character to the emitting states of these complexes.

15

<Figure 6>

## Transient Absorption Spectroscopy

Time-resolved transient absorption (TA) spectra were obtained for MeCN solutions of [Ir($L^{4-6}$)$_2$(bipy)]PF$_6$. Figures 7-9 show the obtained TA spectra, together with the $T_1 \rightarrow S_0$ phosphorescence decay kinetics of the complexes. The appearance of the spectra of [Ir($L^4$)$_2$(bipy)]PF$_6$ and [Ir($L^6$)$_2$(bipy)]PF$_6$ are comparable, with strong positive features at 400 nm < $\lambda$ < 500 nm and 550 nm < $\lambda$ < 700 nm regions, which are the excited state absorption (ESA) bands of the $T_1$ state ($T_1 \rightarrow T_n$ transitions). A bleach at 350 < $\lambda$ < 400 nm is also evident. This general appearance is comparable to that observed previously for Ir(III) 2-phenylquinoxaline complexes.[18] Each feature is associated with similar lifetime characteristics which suggests that each peak relates to the same excitation, ISC process and deactivation. For [Ir($L^4$)$_2$(bipy)]PF$_6$, the triplet state lifetime is 687 ns under $N_2$ atmosphere, the triplet state is quenched by $O_2$ in the air, where experiments show the triplet state lifetime was shortened to 240 ns. Similar results were observed for [Ir($L^5$)$_2$(bipy)]PF$_6$ and [Ir($L^6$)$_2$(bipy)]PF$_6$, where for both complexes the triplet state lifetimes were shortened in aerated solution compared to deaerated solution (Figs 9 and 10).

<Figure 7>
<Figure 8>
<Figure 9>

Interestingly, the TA spectrum of the methoxy-substituted variant [Ir($L^5$)$_2$(bipy)]PF$_6$ is slightly different, with strong positive features (ESA bands) at 400 nm < $\lambda$ < 500 nm and also across the 550 nm < $\lambda$ < 850 nm region. Again, the decay characteristics suggest these features are likely to belong to the same excitation and deactivation

16

processes. To support these studies, the TA spectrum of $[Ir(\mathbf{L^4})_2(bipy)]^+$ was successfully simulated (Fig. S8, SI) by combining admixtures of positive going TD-DFT ESA simulated spectrum for $T_n - T_1$ (n = 1-30) transitions with negative going contributions from a ground state bleach (the negative going UV-vis absorption spectrum) and small contributions of luminescence emission. The simulated spectrum is in excellent agreement with that obtained experimentally (Fig. 7).

Unfortunately, despite numerous attempts using varying concentrations of sample and experimental setup, the very short triplet lifetime characteristics of $[Ir(\mathbf{L^{1-3}})(bipy)]PF_6$ at room temperature precluded detailed TA measurements on these species. In contrast to $[Ir(\mathbf{L^{4-6}})_2(bipy)]PF_6$, for $[Ir(\mathbf{L^{1,2b,3}})_2(bipy)]PF_6$ the absorbance at the excitation wavelength was very weak and insufficient excited states were generated at low concentration. However, monitoring the triplet signal at higher concentrations ($7 \times 10^{-5}$ M) enabled their detection, albeit of weak intensity, and the corresponding time-resolved TA spectra are included for qualitative comparison (Figs. S9-11, SI).

## Triplet-Triplet Annihilation Energy Upconversion (TTA-UC)

As highlighted earlier, a relatively small number of transition metal complexes have been investigated as photosensitizers in TTA-UC. Well known cyclometalated Ir(III) complexes typically possess quite weak molar absorption properties in the visible region and thus rely upon UV or blue light excitation and therefore need adaption for TTA-UC purposes.[44] A long lived triplet excited state is also desirable feature of the photosensitizer. Previous work by Zhao has shown that one strategy for addressing these twin challenges is to conjugate organic chromophores to the ligand framework of the Ir(III) complex moiety.[45] The judicious choice of chromophore enhances absorption in the visible region and can facilitate the $^3$MLCT $\leftrightarrow$ $^3$IL equilibrium leading to a large extension in observed lifetime. In our previous work, red emitting Ir(III) photosensitizers based on cyclometalating 2-phenylquinoxaline ligands also achieved very good visible absorption characteristics. And despite rather modest triplet lifetimes *ca.* 2 μs, these Ir(III) complexes demonstrated exceptional performance in TTA-UC (up to 39% efficiency). As discussed earlier, $[Ir(\mathbf{L^{4-6}})_2(bipy)]PF_6$ possess good absorption characteristics in the visible region, but rather

17

short triplet lifetimes. Therefore, we were interested to assess the performance of $[Ir(L^{4-6})_2(bipy)]PF_6$ as sensitizers in TTA-UC experiments.

Firstly, the triplet levels of the three complexes were approximated from the band onset of the low temperature emission spectra. Obtained values of 16530 ($L^4$), 16260 ($L^5$) and 16390 cm$^{-1}$ ($L^6$) compare to the reported triplet state energy of 9,10-diphenylanthracene (DPA)[46] of 14300 cm$^{-1}$ suggesting that forward TTET is feasible, but that back energy transfer is a possibility where $\Delta E \leq 2000$ cm$^{-1}$. Secondly, solution state (deaerated acetonitrile) TTA-UC measurements were conducted using $[Ir(L^{4-6})_2(bipy)]PF_6$ as the photosensitizers and DPA as the annihilator (see Experimental Section for details). In these measurements, 532 nm excitation was utilized which is selective for the long wavelength absorption of the complexes, and primarily correlates with the spin forbidden ($S_0 \rightarrow T_1$) MLCT-based transition. Critically, DPA does not absorb at this excitation wavelength.

<Figure 10>

The spectroscopic representation of the TTA-UC measurements for each complex is shown in Figure 10. It is clear that in each case addition of DPA to the solution of the Ir(III) sensitizer resulted in a quench of the sensitizer phosphorescence at 600-800 nm and an evolution of DPA-based fluorescence at 400-500 nm. Additional data regarding the dependence of TTA-UC upon DPA concentration and excitation power are shown in Figs S12-S17, SI. Upconversion luminescence intensity was shown to reach a plateau at a DPA concentration of 5 × 10$^{-4}$ M. Thus, a photosensitiser/DPA ratio of 1:5 was utilized for the upconversion quantum yield measurements. The upconversion also showed a linear relationship with excitation power density. At a laser power intensity of 76.5 mW cm$^{-2}$, the relative efficiencies of this process were given by upconversion quantum yields ($\Phi_{UC}$) of 6.7%, 2.2% and 1.6% for $[Ir(L^4)_2(bipy)]PF_6$, $[Ir(L^5)_2(bipy)]PF_6$ and $[Ir(L^6)_2(bipy)]PF_6$, respectively. The visual phenomenon of energy upconversion in these systems can be seen in Figure 11 where photographs clearly illustrate the effect of mixing the DPA annihilator into the different solutions of the Ir(III) sensitizers.

<Figure 11>

18

**Conclusions**

A series of structurally related cyclometalated Ir(III) complexes that incorporate substituted 2-(naphthalen-1-yl)quinoline-4-carboxylate and 2-(naphthalen-2-yl)quinoline-4-carboxylate type ligands have been synthesised. The complexes are all red emitters with subtle variance according to ligand structure. A range of spectroscopic and analytical techniques suggest that the position of chelation at the naphthyl unit strongly influences the emission properties, more so than the role of the ligand substituent. Supporting TD-DFT calculations suggest the emission properties are described by a mixture of ligand-centred and MLCT character contributing to the emitting state. Within the series, [Ir(**L**$^{4-6}$)$_2$(bipy)]PF$_6$ possess much more favourable absorption characteristics in the visible region and longer triplet lifetimes. These twin attributes appear to enable [Ir(**L**$^{4-6}$)$_2$(bipy)]PF$_6$ to be operative sensitizers for TTA-UC with efficiencies up to *ca*. 7%. Therefore while these conjugated naphthylquinoline ligands represent a viable strategy to bathochromically shift the absorption and emission properties of the resultant Ir(III) complexes, these species are unexpectedly compromised with respect to their triplet lifetimes under deaerated conditions.

19

## Experimental

All reactions were performed with the use of vacuum line and Schlenk techniques. Reagents were commercial grade and were used without further purification. $^1H$, $^{13}C$ and $^{19}F$ NMR spectra were recorded on a Bruker Avance dpx 400, or 500 MHz spectrometer, and were recorded in $CDCl_3$, $CD_3CN$ or $d^6$-DMSO solutions. $^1H$ and $^{13}C\{^1H\}$ NMR chemical shifts ($\delta$) were determined relative to internal tetramethylsilane, $Si(CH_3)_4$ and are given in ppm. Low-resolution mass spectra were obtained by the staff at Cardiff University. High-resolution mass spectra were carried out by the staff at Cardiff University and the EPSRC National Mass Spectrometry Service at Swansea University, UK. All photophysical data was obtained on a JobinYvon-Horiba Fluorolog-3 spectrometer fitted with a JY TBX picosecond photodetection module in $CHCl_3$ or MeCN solutions. Emission spectra were uncorrected and excitation spectra were instrument corrected. The pulsed source was a Nano-LED configured for 295, 372 or 459 nm output operating at 500 kHz or 1 MHz. Luminescence lifetime profiles were obtained using the JobinYvon–Horiba FluoroHub single photon counting module and the data fits yielded the lifetime values using the provided DAS6 deconvolution software. IR spectra were recorded on an ATR equipped Shimadzu IRAffinity-1 spectrophotometer. UV-vis data were recorded as solutions on a Perkin Elmer Lamda20 spectrophotometer. TTA Energy Upconversion measurements utilized $c$(sensitiser) = $1 \times 10^{-5}$ M, $c$(DPA) = $5 \times 10^{-4}$ M, 20 °C; deaerated MeCN; and the upconversion quantum efficiencies were obtained using Bengal Rose as a standard ($\Phi_F$ = 0.08 in methanol).

## Triplet–triplet annihilation upconversion

A 532 nm continuous wave (CW) diode-pumped solid state laser was used as the excitation light source for the TTA upconversion experiments. The upconverted fluorescence was recorded with a RF 5301PC spectrofluorometer (Shimadzu Ltd., Japan). The mixed solution of triplet energy donor and acceptor were purged with $N_2$ for 15 min before measurement. The upconversion quantum yields were determined with Rose Bengal ($\Phi_F$ = 0.08 in methanol) as the luminescence quantum yield standard. The upconversion quantum yields were calculated with the following equation (Eq. 1), the subscript with 'std' and 'sam' stand for the corresponding

20

parameter for the standard and sample (Eq. x), $\Phi$, A, I and $\eta$ represents the quantum yield, absorbance, integrated photoluminescence intensity and the refractive index, respectively. Factor 2 is used in the equation, thus the maximal upconversion quantum yield should be 100%.

$$\Phi_{\text{UC}} = 2\,\Phi_{\text{std}} \left( \frac{1 - 10^{-A_{\text{std}}}}{1 - 10^{-A_{\text{sam}}}} \right) \left( \frac{I_{\text{sam}}}{I_{\text{std}}} \right) \left( \frac{\eta_{\text{sam}}}{\eta_{\text{std}}} \right)^2 \qquad \text{Eq. 1}$$

Spin statistics predicts that the upconversion quantum yield should be less than 11.1% (given the maximal upconversion quantum yield is 50%). However, the recent studies indicated that the upconversion quantum yields of some systems are up to 30%, because higher spin states can also be involved in the TTA upconversion.[47]

## Nanosecond transient absorption spectroscopy

The nanosecond transient absorption spectra were studied on LP980 Laser Flash Photolysis Spectrometer (Edinburgh Instruments, U.K.). Before the measurements, the sample solution was purged with $N_2$ for 15 min. The spectra were recorded in collinear mode and excited with a nanosecond pulsed laser (Opolette 355II+UV nanosecond pulsed laser, OPOTEK). The typical laser power is ca. 5 mJ per pulse. The data was analyzed with software of L900.

## X-ray crystallography

## Data collection and processing

Suitable crystals were selected and data collected following a standard method,[48] on either a a Rigaku FRE+ diffractometer equipped with VHF Varimax confocal mirrors and an AFC12 goniometer and HyPix 6000 detector, equipped with an Oxford Cryosystems low-temperature device operating at $T = 100(2)$ K (for [Ir(**L³**)₂(bipy)]PF₆ and [Ir(**L⁴**)₂(bipy)]PF₆) or a Rigaku 007HF diffractometer equipped with Varimax confocal mirrors and an AFC11 goniometer and HyPix 6000 detector equipped with an Oxford Cryosystems low-temperature device operating at $T = 100(2)$ K (for [Ir(**L⁶**)₂(bipy)]PF₆).

21

Cell determination, data collection, data reduction, cell refinement and absorption correction were carried out using CrysAlisPro[49] The structures were solved with the ShelXT[50] structure solution program using the Intrinsic Phasing solution method and by using Olex2[51] as the graphical interface. The models were refined with version 2018/3 of ShelXL[52] using Least Squares minimisation.

## DFT studies

All calculations were performed within the Gaussian 09 suite of programmes.[53] Geometry optimisations were carried out without constraints using the DFT//B3LYP level of theory.[54] The Stuttgart-Dresden basis set was used for the iridium atoms,[55] and was invoked with pseudo-potentials for the core electrons, with a 6-31G* basis set for all remaining atoms.[56] All calculations included the use of a polarized continuum model (IEFPCM) approach for the treatment of the MeCN solvent.[57] All stationary point geometries obtained by DFT method were confirmed through harmonic vibrational frequency calculations

All absorption spectra predictions, orbitals and other ground state properties were computed using the ground state minimum energy geometry. Excitation energies (absorption spectra predictions) were computed in the same manner as ground state properties, but using the long range corrected CAM-B3LYP functional for improved accuracy. For the prediction of emission energies, the triplet state was allowed to relax to its optimal geometry, prior to single point energy calculations of the ground state at this set of geometric parameters. Molecular orbital decomposition was performed using the GaussSum package. [58]

22

Notes and references ‡ CCDC 2023982, 2023983, 2023984 contains supplementary X-ray crystallographic data for [Ir($L^3$)$_2$(bipy)]PF$_6$, [Ir($L^4$)$_2$(bipy)]PF$_6$, and [Ir($L^6$)$_2$(bipy)]PF$_6$ respectively. This data can be obtained free of charge via http://www.ccdc.cam.ac.uk/conts/retrieving.html, or from the Cambridge Crystallographic Data Centre, Union Road, Cambridge, CB2 1EZ; fax(+44) 1223-336-033 or email: deposit@ccdc.cam.ac.uk.

Corresponding Authors: Prof. Simon J. A. Pope: E-mail: PopeSJ@cardiff.ac.uk Dr Joseph M. Beames: E-mail: BeamesJ@cardiff.ac.uk

Accepted Manuscript

23

# Figures and Captions
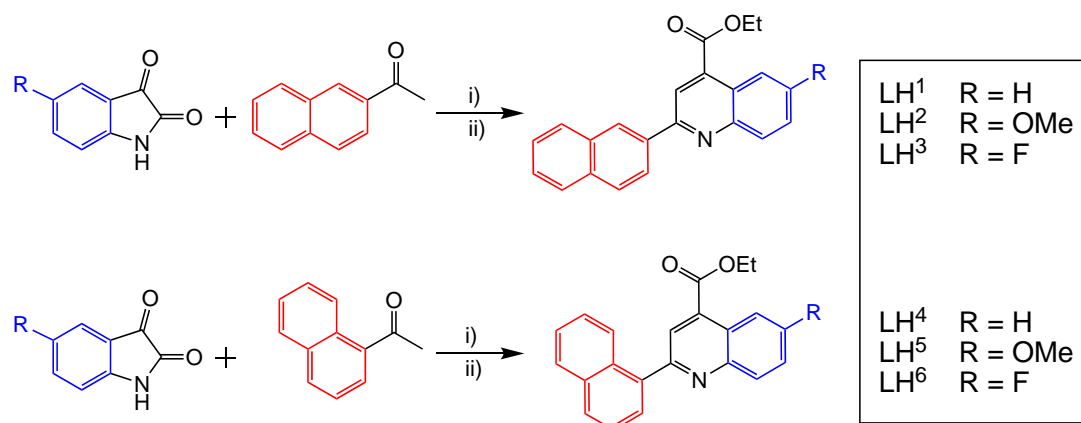


**Scheme 1**. Synthesis of the ligands: (i) NaOH, EtOH; (ii) EtOH, HCl.



$[Ir(L^{1,3})_2(bipy)]PF_6$ $[Ir(L^{2b})_2(bipy)]PF_6$ $[Ir(L^{4-6})_2(bipy)]PF_6$
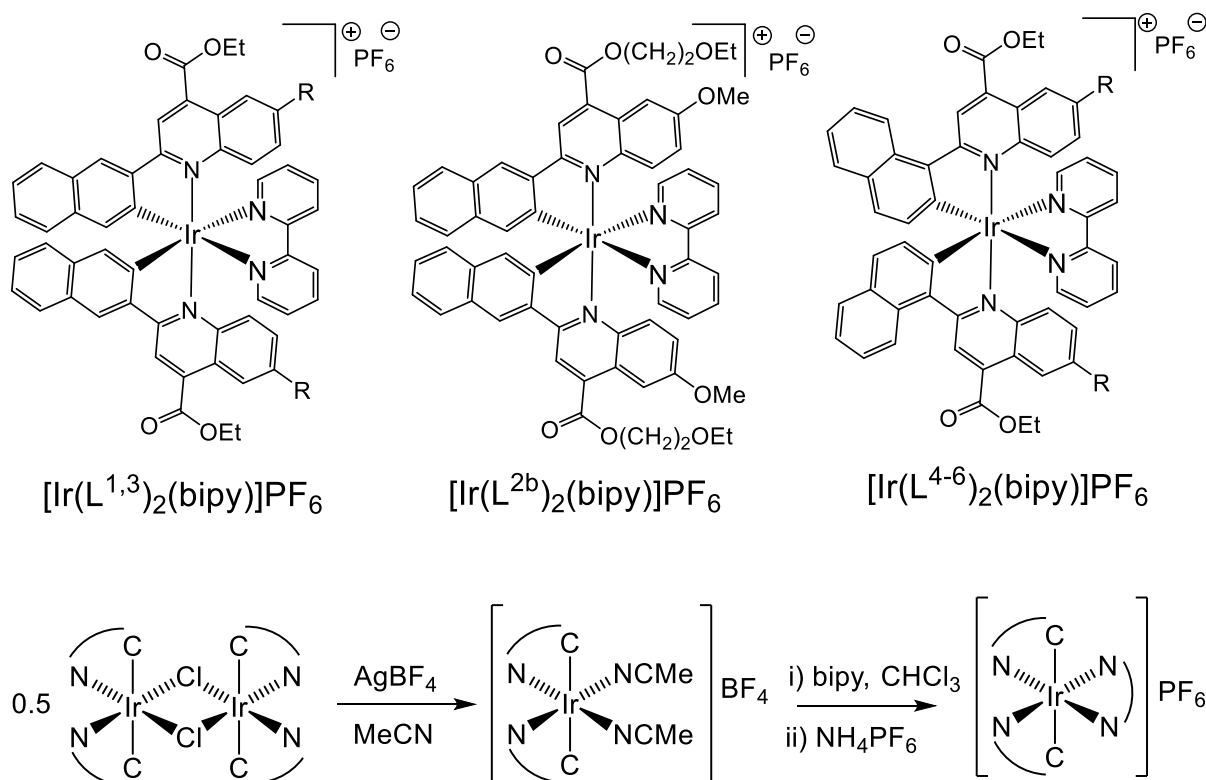


**Scheme 2. Top:** Structures of the synthesized cationic Ir(III) complexes. **Bottom**: general synthetic route.

24

:
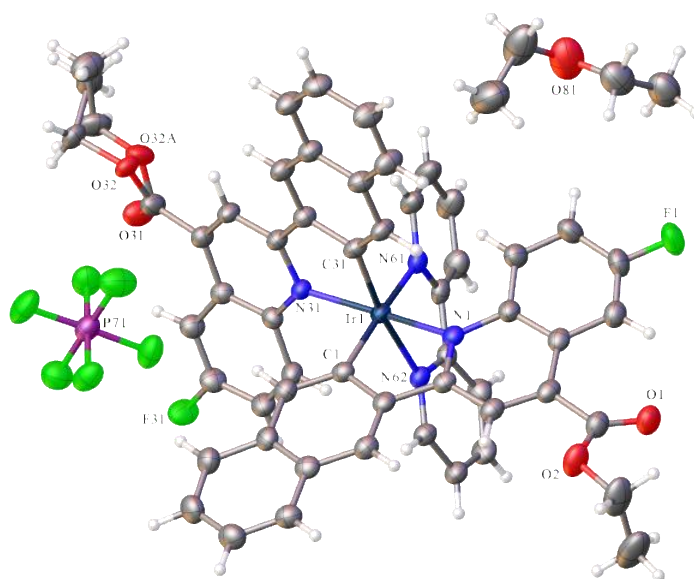
**Figure 1.** X-ray structure of [Ir(**L³**)₂(bipy)]PF₆. Note the disorder on one of the ester groups.
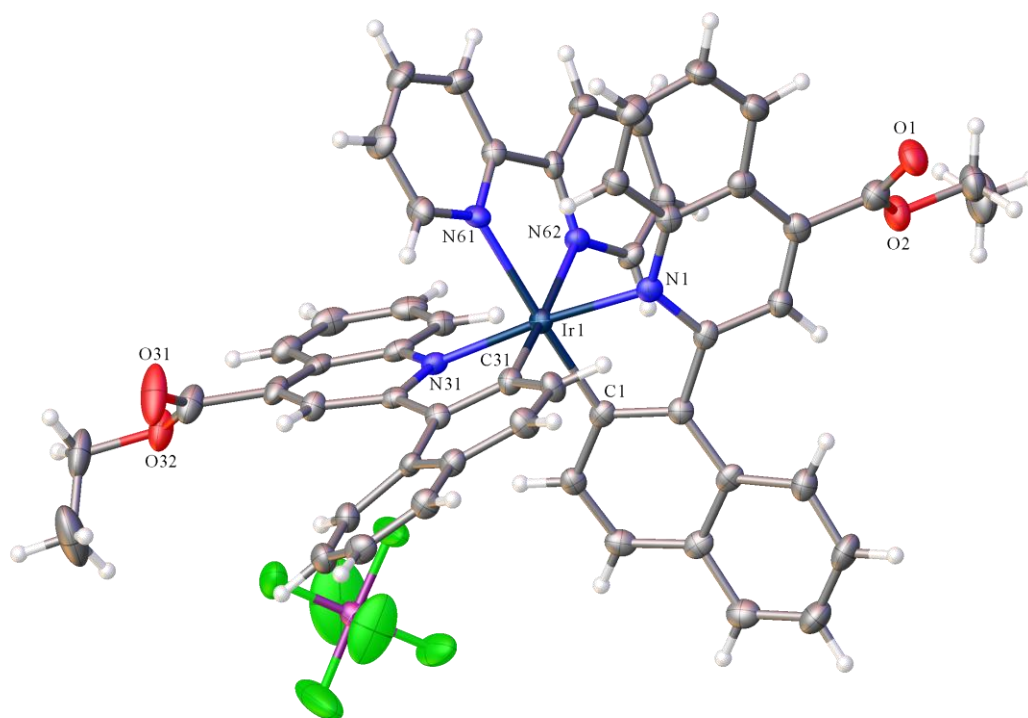


**Figure 2.** X-ray structure of [Ir(**L⁴**)₂(bipy)]PF₆. Solvent not shown. Note the intraligand distortion.
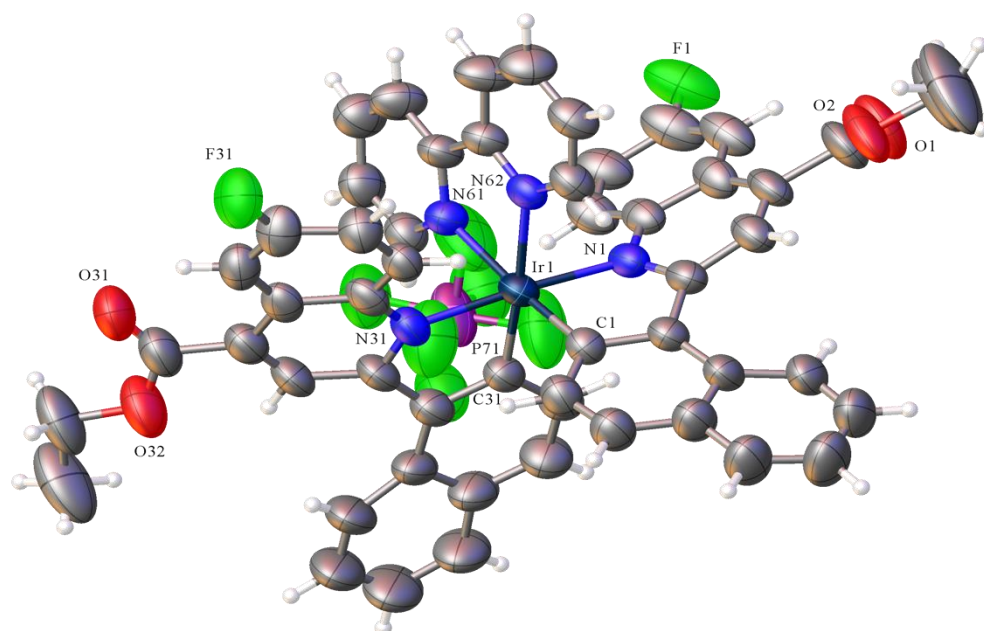
25

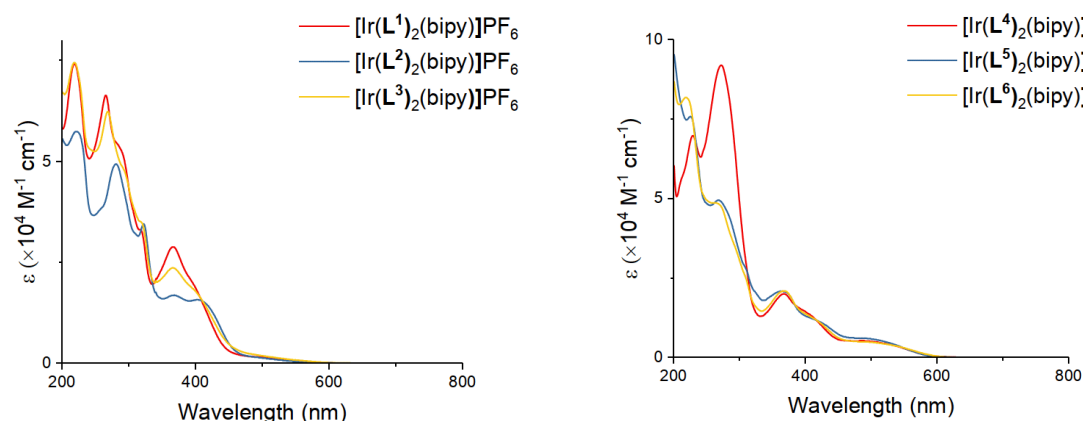**Figure 3.** X-ray structure of [Ir(**L⁶**)₂(bipy)]PF₆. Solvent not shown.

26

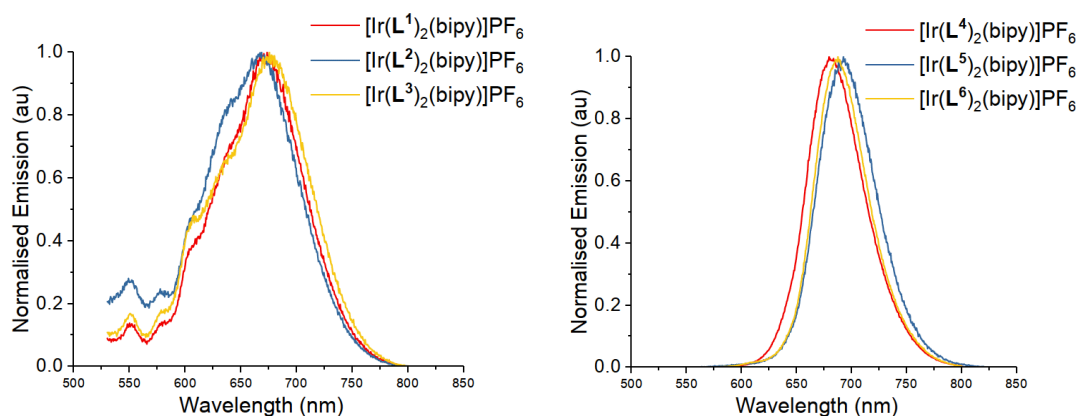**Figure 4**. UV-vis. absorption spectra of the complexes ($10^{-5}$ M, MeCN).



**Figure 5**. Normalized room temperature luminescence spectra of the complexes (aerated MeCN; $\lambda_{ex}$ = 510 nm).
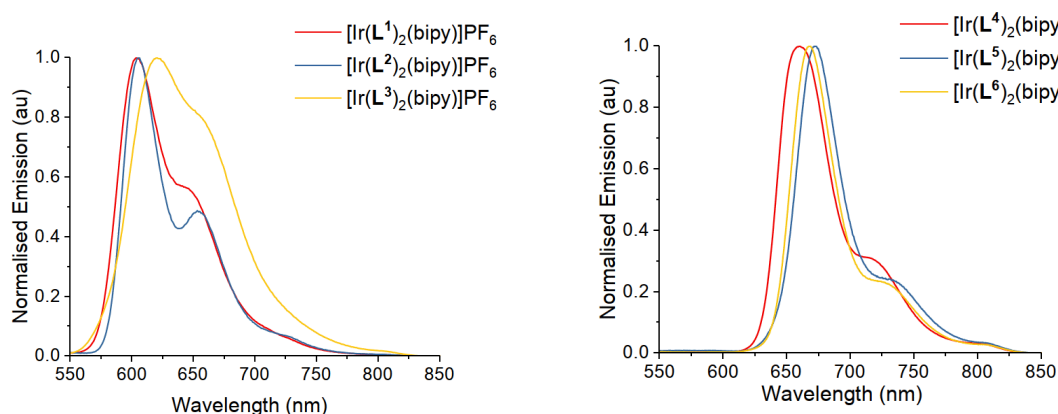


**Figure 6**. Luminescence spectra of the complexes recorded as a frozen glass (1:4, MeOH/EtOH) ($\lambda_{ex}$ = 510 nm).
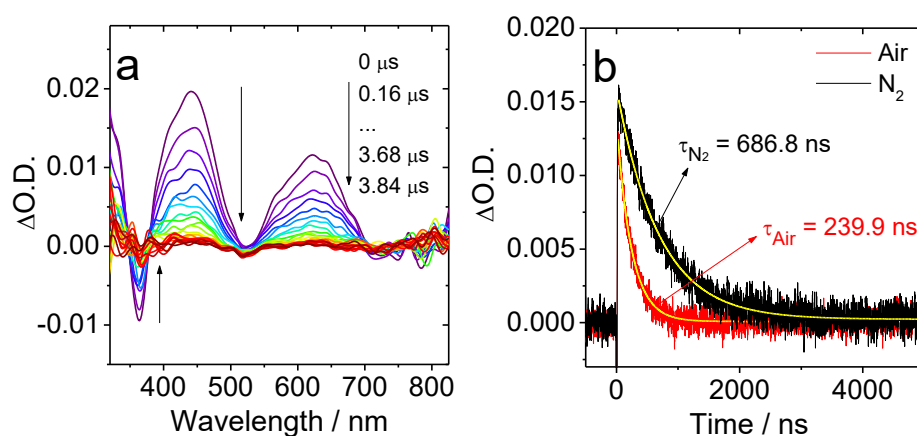
27

**Figure 7**. (a) Nanosecond time-resolved transient absorption spectra of compound [Ir($L^4$)$_2$(bipy)]PF$_6$ upon pulsed laser excitation in deaerated acetonitrile ($\lambda_{ex}$ = 510 nm, $c$ = 5 × 10$^{-5}$ M) and (b) decay trace of compound [Ir($L^4$)$_2$(bipy)]PF$_6$ at 625 nm in acetonitrile ($c$ = 5 × 10$^{-5}$ M) under air and N$_2$ atmosphere, respectively, 20 °C.



**Figure 8**. (a) Nanosecond time-resolved transient absorption spectra of compound [Ir($L^5$)$_2$(bipy)]PF$_6$ upon pulsed laser excitation in deaerated acetonitrile ($\lambda_{ex}$ = 510 nm, $c$ = 5 × 10$^{-5}$ M) and (b) decay trace of compound [Ir($L^5$)$_2$(bipy)]PF$_6$ at 645 nm in acetonitrile ($c$ = 5 × 10$^{-5}$ M) under air and N$_2$ atmosphere, respectively, 20 °C.

28

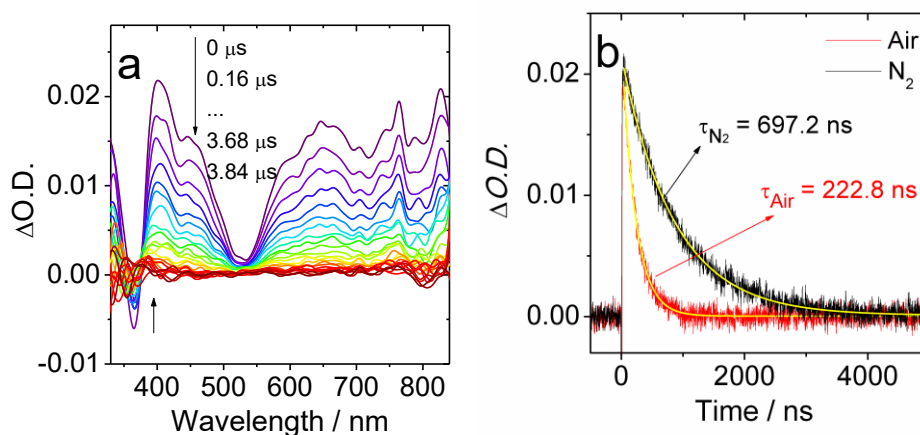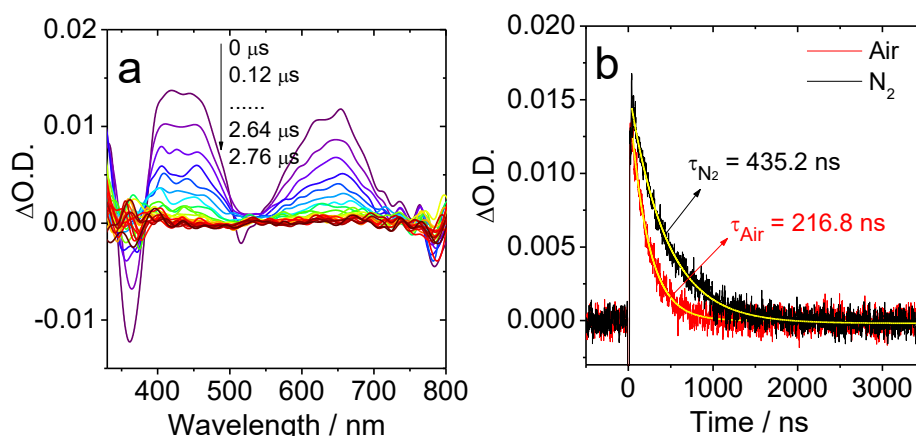**Figure 9.** (a) Nanosecond time-resolved transient absorption spectra of compound [Ir($L^6$)$_2$(bipy)]PF$_6$ upon pulsed laser excitation in deaerated acetonitrile ($\lambda_{ex}$ = 510 nm, $c$ = 5 × 10$^{-5}$ M) and (b) decay trace of compound [Ir($L^6$)$_2$(bipy)]PF$_6$ at 645 nm in acetonitrile ($c$ = 5 × 10$^{-5}$ M) under air and N$_2$ atmosphere, respectively, 20 °C.
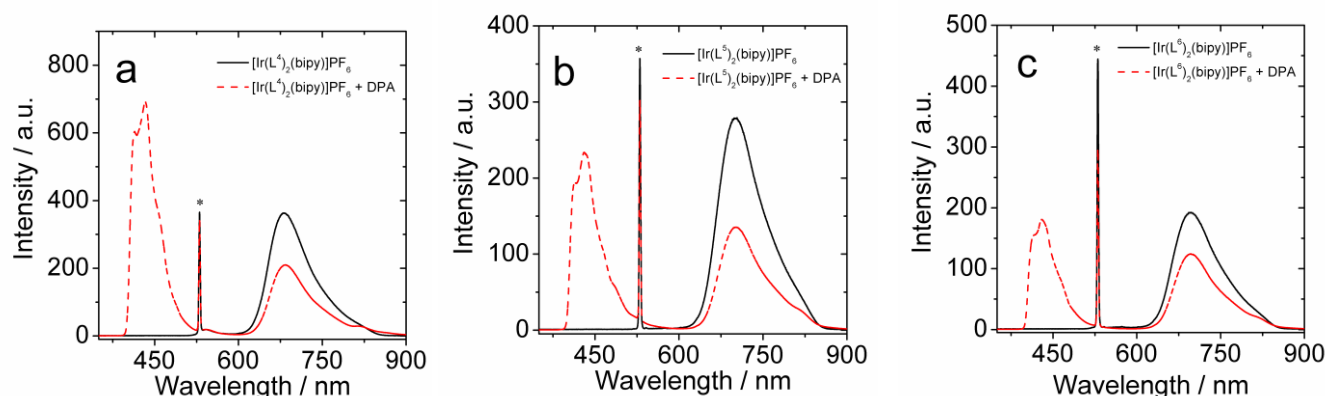


**Figure 10.** Triplet-triplet annihilation upconversion emission spectra with the photosensitizers, (a) [Ir($L^4$)$_2$(bipy)]PF$_6$, (b) [Ir($L^5$)$_2$(bipy)]PF$_6$, and (c) [Ir($L^6$)$_2$(bipy)]PF$_6$, in deaerated acetonitrile where DPA was used as the annihilator. Excitation was achieved with a continuous laser at $\lambda$ = 532 nm (power density of 5.6 mW) under a deaerated atmosphere. $c$(sensitizer) = 1 × 10$^{-5}$ M, $c$(DPA) = 5 × 10$^{-4}$ M, 20 °C. The asterisks indicate the scattered laser signal.

29

**Figure 11**. Photographs of the emission of the selected triplet sensitizers and their upconversion with DPA in deaerated acetonitrile. Excitation was achieved with a continuous laser at $\lambda$ = 532 nm (power density of 5.6 mW) under a deaerated atmosphere. $c$(sensitizer) = 1 × $10^{-5}$ M, $c$(DPA) = 5 × $10^{-4}$ M, 20 °C. The photographs were taken without any filters.

## TOC text

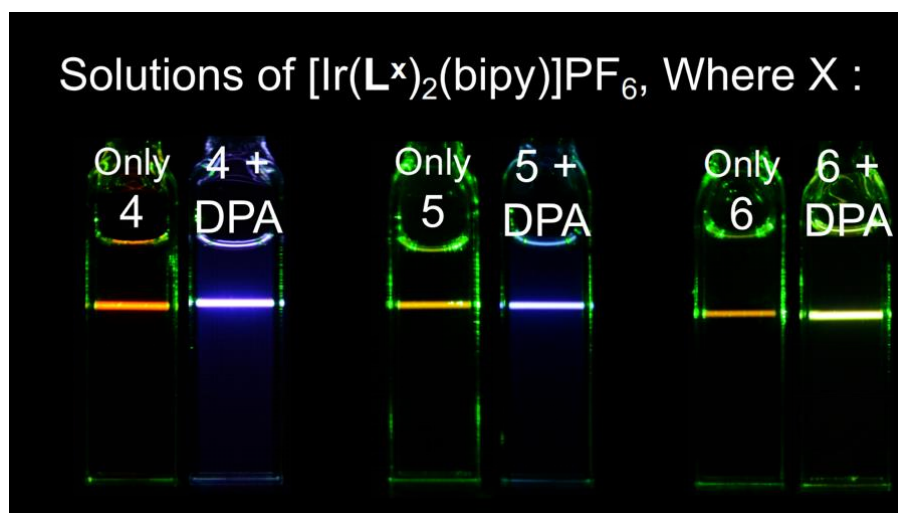A series of substituted naphthylquinolines have been synthesized and investigated as cyclcometalating ligands for Ir(III). The resultant complexes were shown to be emissive in the deep red region and several identified as viable photosensitisers for triplet-triplet annihilation upconversion.

## References

[1] Iridium(III) in Optoelectronic and Photonics Applications; E. Zysman-Colman, Ed.; John Wiley & Sons, Inc: Chichester, West Sussex, 2017.

[2] a) K.K-W. Lo, D.C-M. Ng, C-K. Chung, *Organometallics* **2001**, *20*, 4999; b) Q. Zhao, C. Huang, F. Li, *Chem. Soc. Rev*. **2011**, *40*, 2508; c) E. Baggaley, M.R. Gill, N.H. Green, D. Turton, I.V. Sazanovich, S.W. Botchway, C. Smythe, J.W. Haycock, J. A. Weinstein, J. A. Thomas, *Angew. Chem. Int. Ed*. **2014**, *53*, 3367; d) M.P. Coogan, V. Fernandez-Moreira, *Chem. Commun.* **2014**, *50*, 384; e) L.K. McKenzie, I.V. Sazanovich, E. Baggaley, M. Bonneau, V. Guerchais, J.A.G. Williams, J.A. Weinstein, H.E. Bryant, *Chem. Eur. J.* **2017**, *23*, 234; f) E. Baggely, J.A. Weinstein, J.A. Williams, *Struct. Bonding* **2015**, *165*, 205.

30

3 a) S. Lamansky, P. Djurovich, D. Murphy, F. Abdel-Razzaq, H-E. Lee, C. Adachi, P.E. Burrows, S.R. Forrest, M.E. Thompson, *J. Am. Chem. Soc.* **2001**, *123*, 4304; b) D. Ma, R. Liu, C. Zhang, Y. Qiu, L. Duan, *ACS Photonics* **2018**, *5*, 3428; c) D. Ma, C. Zhang, R. Liu, Y. Qiu, L. Duan, *ACS Appl. Mater. Interfaces* **2018**, *10*, 29814; d) D. Tordera, A. Pertegas, N.M. Shavaleev, R. Scopelliti, E. Orti, H.J. Bolink, E. Baranoff, M. Gratzel, M.K. Nazeeruddin, *J. Mat. Chem.* **2012**, *22*, 19264; e) I.N. Mills, J.A. Porras, S. Bernhard, *Acc. Chem. Res.* **2018**, *15*, 352.

4 a) C.K. Prier, D.A. Rankic, D.W.C. MacMillan, *Chem. Rev.* **2013**, *113*, 5322; b) Z. Zuo, D.T. Ahneman, L. Chu, J.A. Terrett, A.G. Doyle, D.W.C. MacMillan, *Science* **2014**, *345*, 437; A.J. Hallet, N. White, W. Wu, X. Cui, P.N. Horton, S.J. Coles, J. Zhao, S.J.A. Pope, *Chem. Commun.* **2012**, *48*, 10838.

5 Y. Li, N. Dandu, R. Liu, L. Hu, S. Kilina, W. Sun, *ACS Appl. Mater. Interfaces* **2013**, *5*, 6556.

6 a) S.J. Sheet, B. Sen. S. Khatua, *Inorg. Chem.* **2019**, *58*, 3635; b) W.H-T. Law, K-K. Leung, L.C-C. Lee, C-S. Poon, H-W. Liu, K.K-W. Lo, *ChemMedChem.* **2014**, *9*, 1316; c) K.W-W. Lo, S.P-Y. Li, K.Y. Zhang, *New J. Chem.* **2011**, *35*, 265.

7 A.F. Henwood, E. Zysman-Colman, *Chem. Commun.* **2016**, *53*, 807

8 a) P-N. Lai, T.S. Teets, *Chem. Eur. J.* **2019**, *25*, 6026; b) P-N. Lai, Alam, M.K. Brysacz, N.A. Ayoub, T.G. Gray, J. Bao, T.S. Teets, *J. Am. Chem. Soc.* **2018**, *140*, 10198.

9 a) T.N. Singh-Rachford, F.N. Castellano, *Coord. Chem. Rev.* **2010**, *254*, 2560; b) X. Guo, Y. Liu, Q. Chen, D. Zhao, Y. Ma, *Adv. Opt. Mat.* **2018**, *6*, 1700981; c) C. Kerzig, O.S. Wenger, *Chem. Sci.* **2018**, *9*, 6670; d) J. Zhao, W. Wu, J. Sun, S. Guo, *Chem. Soc. Rev.* **2013**, *42*, 5323; d) C.E. McCusker, F.N. Castellano, *Top. Curr. Chem.* **2016**, *374*, 19; e) F.N. Castellano, C.E. McCusker, *Dalton Trans.* **2015**, *44*, 17906.

10 R.R. Islangulova, D.V. Kozlov, F.N. Castellano, *Chem. Commun.* **2005**, 3776.

11 K.A. El Roz, F.N. Castellano, *Chem. Commun.* **2017**, *53*, 11705.

12 T.N. Singh-Rachford, A. Nayak, M.L. Muro-Small, S. Goeb, M.J. Therien, F.N. Castellano, *J. Am. Chem. Soc.* **2010**, *132*, 14203.

13 a) C.E. McCusker, F.N. Castellano, *Chem. Commun.* **2013** *49*, 3537; b) C.E. McCusker, F.N. Castellano, *Inorg. Chem.* **2015**, *54*, 6035; c) M.S. Lazorski, F.N. Castellano, *Polyhedron* **2014**, *82*, 57.

31

[14] d) X. Chu, M. Guan, L. Niu, Y. Zeng, Y. Li, Y. Zhang, Z. Zhu, B. Wang, *ACS Appl. Mater. Interfaces* **2014**, *6*, 19011;

[15] See also: P. Duan, N. Yanai, N. Kimizuka, *Chem. Commun.* **2014**, *50*, 13111.

[16] a) J. Peng, X. Jiang, X. Guo, D. Zhao, Y. Ma, *Chem. Commun.* **2014**, *50*, 7828; b) X. Jiang, X. Guo, J. Peng, D. Zhao, Y. Ma, *ACS Appl. Mater. Interfaces* **2016**, *8*, 11441; c) X. Guo, Q. Chen, Y. Tong, Y. Li, Y. Liu, D. Xhao, Y. Ma, *J. Phys. Chem. A*, **2012**, *122*, 6963.

[17] a) X. Yi, P. Yang, D. Huang, J. Zhao, *Dyes and Pigments* **2013**, *96*, 104; b) J. Sun, W. Wu, J. Zhao, *Chem. Eur. J.* **2012**, *18*, 8100; c) J. Sun, F. Zhong, X. Yi, J. Zhao, *Inorg. Chem.* **2013**, *52*, 6299; d) L. Ma, H. Guo, Q. Li, S. Guo, J. Zhao, *Dalton Trans.* **2012**, *41*, 10680; e) X. Yi, C. Zhang, S. Guo, J. Ma, J. Zhao, *Dalton Trans.* **2014**, *43*, 1672; f) Y. Lu, J. Wang, N. McGoldrick, X. Cui, J. Zhao, C. Caverly, B. Twamley, G.M.O Maille, B. Irwin, R. Conway-Kenny, S.M. Draper *Angew. Chem. Int. Ed.* **2016**, *55*, 14688; g) Y. Lu, N. McGoldrick, F. Murphy, B. Twamley, X. Cui, C. Delaney, G.M. O Maille, J. Wang, J. Zhao, S.M. Draper, *Chem. Eur. J.* **2016**, *22*, 11349.

[18] K.A. Phillips, T.M. Stonelake, K. Chen, Y. Hou, J. Zhao, S.J. Coles, P.N. Horton, S.J. Keane, E.C. Stokes, I.A. Fallis, A.J. Hallett, S.P. O'Kell, J.B. Beames, S.J.A. Pope, *Chem. Eur. J.* **2018**, *24*, 8577.

[19] a) E.E. Langdon-Jones, A.J. Hallett, J.D. Routledge, D.A. Crole, B.D. Ward, J.A. Platts, S.J.A. Pope, *Inorg. Chem.* **2013**, *52*, 448; b) T.M. Stonelake, K.A. Phillips, H.Y. Otaif, Z.C. Edwardson, P.N. Horton, S.J. Coles, J.M. Beames, S.J.A. Pope, *Inorg. Chem.* **2020**, *59*, 2266

[20] See also: a) D. Schneidenbach, S. Ammermann, M. Debeaux, A, Freund, M. Zollner, C. Daniliuc, P.G. Jones, W. Kowalsky, H-H. Johannes, *Inorg. Chem.* **2010**, *49*, 397; b) Y-M. Jing, F-Z. Wang, Y-X. Zheng, J-L. Zuo, *J. Mater. Chem. C* **2017**, *5*, 3714; c) W. Sun, C. Pei, T. Lu, P. Cui, Z. Li, C. McCleese, Y. Fang, S. Kilina, Y. Song, C. Burda, C. *J. Mater. Chem. C* **2016**, *4*, 5059; d) K. Tani, H. Fujii, L. Mao, H. Sakurai, T. Hirao, *Bull. Chem. Soc. Jap.* **2007**, *80*, 783.

[21] A. Tsuboyama, H. Iwawaki, M. Furugori, T. Mukaide, J. Kamatani, S. Igawa, T. Moriyama, S. Miura, T. Takiguchi, S. Okada, M. Hoshino, K. Ueno, *J. Am. Chem. Soc.* **2003**, *125*, 12971.

[22] Y.J. Su, H.L. Huang, C.L. Li, C.H. Chien, Y.T. Tao, P.T. Chou, S. Datta, R.S. Liu, *Adv. Mater.* **2003**, *15*, 884; C.L. Li, Y.J. Su, Y.T. Tao, P.T. Chou, C.H. Chien, C.C.

32

:

Cheng, R.S. Liu, *Adv. Funct. Mater.* **2005**, *15*, 387; S. Huo, J.C. Deaton, M. Rajeswaran, W.C. Lenhart, *Inorg. Chem.* **2006**, *45*, 3155.

23 A. Tsuboyama, H. Iwawaki, M. Furugori, T. Mukaide, J. Kamatani, S. Igawa, T. Moriyama, S. Miura, T. Takiguchi, S. Okada, M. Hoshino, K. Ueno *J. Am. Chem. Soc.* **2003**, *125*, 12971

24 (a) J. Guo, J. Zhou, G. Fu, Y. He, W. Li, X. Lu, *Inorg. Chem. Commun.* **2019**, *101*, 69; (b) C.-J. Li, S.-Y. Yin, H.-P. Wang, Z.-W. Wei, M. J. Pan, *Photochem. Photobiol., A* **2019**, *379*, 99; (c) H.-Y. Chen, C.-H. Yang, Y. Chi, Y.-M. Cheng, Y.-S. Yeh, P.-T. Chou, H.-Y. Hsieh, C.-S. Liu, S.-M. Peng, G.-H. Lee, *Can. J. Chem.* **2006**, *84*, 309

25 A. Tsuboyama, H. Iwawaki, M. Furugori, T. Mukaide, J. Kamatani, S. Igawa, T. Moriyama, S. Miura, T. Takiguchi, S. Okada, M. Hoshino, K. Ueno, *J. Am. Chem. Soc.* **2003**, *125*, 12971.

26 S. Lamansky, P. Djurovich, D. Murphy, F. Abdel-Razzaq, H-E. Lee, C. Adachi, P.E. Burrows, S.R. Forrest, M.E. Thompson *J. Am. Chem. Soc.* **2001**, *123*, 4304

27 P.A. Scattergood, A.M. Ranieri, L. Charalambou, A. Comia, D.A.W. Ross, C.R. Rice, S.J.O. Hardman, J-L. Heully, I.M. Dixon, M. Massi, F. Alary, P.I.P. Elliott, *Inorg. Chem.* **2020**, *59*, 1785.

28 R. Bevernaegie, S.A.M. Wehlin, E.J. Piechota, M. Abraham, C. Philouze, G.J. Meyer, B. Elias, L. Troian-Gautier, *J. Am. Chem. Soc.* **2020**, *142*, 2732.

29 X-F. Ma, J-C. Xia, Z-P. Yan, X-F. Luo, Z-G. Wu, Y-X. Zheng, W-W. Zhang, *J. Mat. Chem. C* **2019**, *7*, 2570.

30 E. Kabir, Y. Wu, S. Sittel, B-L. Nguyen, T.S. Teets, *Inorg. Chem. Front.* **2020**, *7*, 1362.

31 a) J.D. Routledge, A.J. Hallett, J.A. Platts, P.N. Horton, S.J. Coles, S.J.A. Pope, *Eur. J. Inorg. Chem.* **2012**, 4065;  b) J.E. Jones, R.L. Jenkins, R.S. Hicks, A.J. Hallett, S.J.A. Pope, *Dalton Trans.* **2012**, *41*, 1072; c) J.A. Lowe, O.J. Stacey, P.N. Horton, S.J. Coles, S.J.A. Pope, *J. Organomet. Chem.* **2016**, *805*, 87; d) O.J. Stacey, J.A. Platts, S.J. Coles, P.N. Horton, S.J.A. Pope, *Inorg. Chem.* **2015**, *54*, 6528; e) O.J. Stacey, B.D. Ward, S.J. Coles, P.N. Horton, S.J.A. Pope, *Dalton Trans.* **2016**, *45*, 10297.

32 For example, a) D. Li, X. Yan, Y. Hu, Y. Liu, R. Guo, M. Liao, B. Shao, Q. Tang, X. Guo, R. Chai, Q. Zhang, M. Tang, *ACS Biomaterials Sci. Eng.* **2019**, *5*, 1561; b) A.H. Day, M.H. Ubler, H.L. Best, E. Lloyd-Evans, R.J. Mart, I.A. Fallis, R.K. Allemann,

33

E.A.H. Al-Wattar, N.I. Keymer, N.J. Buurma, S.J.A. Pope, *Chem. Sci.* **2020**, *11*, 1599.

[33] Z. Li, P. Cui, C. Wang, S. Kilina, W. Sun, *J. Phys. Chem. C* **2014**, *118*, 28764

[34] W. Pfitzinger, *J. Prakt. Chem.* **1888**, *36*, 582

[35] J.A. Knight, H.K. Porter, P.K. Calaway, *J. Am. Chem. Soc.* **1944**, *66*, 1893.

[36] M.G.A. Shvekhgeimer, *Chemistry of Heterocyclic Compounds* **2004**, *40*, 257.

[37] See Experimental section.

[38] M. Nonoyama, *Bull. Chem. Soc. Jap.* **1974**, *47*, 767.

[39] R.A. Smith,; E.C. Stokes, E.E. Langdon-Jones, J.A. Platts, B.M. Kariuki, A.J. Hallett, S.J.A. Pope, *Dalton Trans.* **2013**, *42*, 10347.

[40] a) A.B. Tamayo, B.D. Alleyne, P.I. Djurovich, S. Lamansky, I. Tsyba, N.M. Ho, R. Bau, M.E. Thompson, *J. Am. Chem. Soc.* **2003**, *125*, 7377; b) S. Lamansky, P. Djurovich, D. Murphy, F. Abdel-Razzaq, R. Kwong, I. Tsyba, M. Bortz, B. Mui, R. Bau, M.E. Thompson, *Inorg. Chem.* **2001**, *40*, 1704; c) M.C. Colombo, T.C. Brunold, T. Riedener, H.U. Gudel, M. Fortsch, H-B. Burgi, *Inorg. Chem.* **1994**, *33*, 545

[41] M. Llunell, D. Casanova, J. Girera, P. Alemany, S. Alvarez, SHAPE, Continuous Shape Measures Calculation, version 2.0; Universitat de Barcelona: Barcelona, Spain, 2010

[42] a) R. Liu, N. Dandu, J. Chen, Y. Li, Z. Li, S. Liu, C. Wang, S. Kilina, B. Kohler, W. Sun, *J. Phys. Chem. C* **2014**, *118*, 23233; b) H. Kuo, Y. Chen, L. Devereux, C. Wu, M. Fox, C. Kuei, Y. Chi, G. Lee, *Adv. Mat.* **2017**, *29*, 1702464; c) L. Wang, P. Cui, S. Kilina, W. Sun, *J. Phys. Chem. C* **2017**, *121*, 5719.

[43] A. Juris, V. Balzani, F. Barigelletti, S. Campagna, P. Belser, A. von Zelewsky, *Coord. Chem. Rev.* **1988**, *84*, 85.

[44] For example, Q. Zhao , F. Li , S. Liu , M. Yu , Z. Liu , T. Yi , C. Huang , *Inorg. Chem.* **2008**, 47, 9256.

[45] J. Sun, W. Wu, H. Guo, J. Zhao, *Eur. J. Inorg. Chem.* **2011**, 3165.

[46] J.S. Brinen, J.G. Koren, *Chem. Phys. Lett.* **1968**, *2*, 671.

34

:

[47] Y.Y. Cheng, B. Fuckel, T. Khoury, R.G.C. R. Clady, M.J.Y. Tayebjee, N.J. Ekins-Daukes, M.J. Crossley, T.W. Schmidt, *J. Phys. Chem. Lett.* **2010**, *1*, 1795.

[48] S.J. Coles, P.A. Gale, *Chem. Sci.* **2012**, *3*, 683.

[49] CrysAlisPro Software System, Rigaku Oxford Diffraction, **2018.**

[50] G.M. Sheldrick, *Acta Cryst.* **2015**, *A71*, 3.

[51] O.V. Dolomanov, L.J. Bourhis, R.J. Gildea, J.A.K. Howard, H. Puschmann, *J. Appl. Cryst.* **2009**, *42*, 339-341

[52] G.M. Sheldrick, *Acta Cryst.* **2015**, *C27*, 3.

[53] M. J. Frisch, G. W. Trucks, H. B. Schlegel, G. E. Scuseria, M. A. Robb, J. R. Cheeseman, G. Scalmani, V. Barone, G. A. Petersson, H. Nakatsuji, X. Li, M. Caricato, A. Marenich, J. Bloino, B. G. Janesko, R. Gomperts, B. Mennucci, H. P. Hratchian, J. V. Ortiz, A. F. Izmaylov, J. L. Sonnenberg, D. Williams-Young, F. Ding, F. Lipparini, F. Egidi, J. 33 Goings, B. Peng, A. Petrone, T. Henderson, D. Ranasinghe, V. G. Zakrzewski, J. Gao, N. Rega, G. Zheng, W. Liang, M. Hada, M. Ehara, K. Toyota, R. Fukuda, J. Hasegawa, M. Ishida, T. Nakajima, Y. Honda, O. Kitao, H. Nakai, T. Vreven, K. Throssell, J. A. Montgomery, Jr., J. E. Peralta, F. Ogliaro, M. Bearpark, J. J. Heyd, E. Brothers, K. N. Kudin, V. N. Staroverov, T. Keith, R. Kobayashi, J. Normand, K. Raghavachari, A. Rendell, J. C. Burant, S. S. Iyengar, J. Tomasi, M. Cossi, J. M. Millam, M. Klene, C. Adamo, R. Cammi, J. W. Ochterski, R. L. Martin, K. Morokuma, O. Farkas, J. B. Foresman, and D. J. Fox, Gaussian 09, Revision C.01. Gaussian, Inc., Wallingford CT, 2016.

[54] a) A.D. Becke, *J. Chem. Phys.* **1993**, *98*, 5648; b) C. Lee, W. Yang, R.G. Parr, *Phys. Rev. B* **1988**, *37*, 785.

[55] D. Andrae, U. Haeussermann, M. Dolg, H. Stoll, H. Preuss, *Theor. Chem. Acc.* **1990**, *77*, 123.

[56] a) R. Ditchfield, W.J. Hehre, J.A. Pople, *J. Chem. Phys.* **1971**, *54*, 724; b) W. J. Hehre, R. Ditchfield, J.A. Pople, *J. Chem. Phys.* **1972**, *56*, 2257; c) P. C. Hariharan, J. A. Pople, *Theor. Chem. Acc.* **1973**, *28*, 213.

[57] J. Tomasi, B. Mennucci, R. Cammi, *Chem. Rev.* **2005**, *105*, 2999.

[58] N. M. O'Boyle, A. L. Tenderholt, K. M. Langner, *J. Comput. Chem.* **2008**, *29*, 839.

35